

Analysis of the Indoor Broadband Power-Line Noise Scenario

José Antonio Cortés, Luis Díez, Francisco Javier Cañete, and Juan José Sánchez-Martínez

Abstract—Indoor broadband power-line noise is composed of three main terms: impulsive components, narrowband interferences, and background noise. Most impulsive components have a cyclostationary behavior. However, while some of them consist of impulses of considerable amplitude, width, and repetition rates of 50/100 Hz (in Europe), others have lower amplitude and shorter width but repetition rates of up to hundreds of kilohertz. Classical studies compute statistics of the impulse characteristics without taking into account these significant differences. This paper presents a detailed analysis of these noise terms with a clear distinction between their constituent terms. A classification of the narrowband interferences according to their power spectral density and their statistical behavior is also given. Finally, the instantaneous power spectral density of the background noise and its probability distribution are investigated. Some of the results presented in this paper are available for download from the web site http://www.plc.uma.es/index_eng.htm.

Index Terms—Background noise, broadband power-line communications, impulsive noise, narrowband interferences.

I. INTRODUCTION

IN THE LAST decade, there has been increasing interest in the use of the power-line network for broadband communications purposes. In a first instance, the utilization of low-voltage distribution lines as a last-mile technology attracted significant attention from utility companies. However, strong competition from digital subscriber lines (DSL) and cable services has discouraged the deployment of outdoor power line communications (PLC) systems in most developed countries. Paradoxically, this high penetration of DSL services has widened the possibilities of indoor PLC applications. Since the objective of these systems is to utilize the in-building power grid for computer and entertainment equipment interconnections, they are an appealing solution for the distribution of triple play services in small offices and homes.

As a result of the considerable research effort carried out in the last years, there is a good understanding of the indoor PLC channel response characteristics in the frequency band up to 30 MHz [1], [2] and appropriate models for obtaining representative frequency responses have been proposed [3]–[5]. On the contrary, the work dealing with power-line noise characterization and modeling is much smaller [2], [4], [6]–[9]. Broadband

power-line noise does not with certainty follow the classical additive white Gaussian noise (AWGN) model. It has two main origins: noise generated by the electrical devices connected to the power grid and external noise coupled to the indoor network via radiation or via conduction. It is composed of the following terms [7]:

- 1) *Impulsive noise*: This comprises different components that can be also classified according to:
 - a) *Periodic impulsive noise synchronous with the mains*: It is a cyclostationary noise, synchronous with the mains and with a frequency of 50/100 Hz in Europe. It is commonly originated by silicon controlled rectifiers in power supplies.
 - b) *Periodic impulsive noise asynchronous with the mains*: This has been traditionally considered to be formed by periodic impulses with rates between 50 and 200 kHz. However, repetition rates outside this range have been found in the measurements accomplished in this work. Moreover, in addition to these high repetition frequencies, this type of noise also exhibits an underlying period equal to the mains one, which allows us to categorize it as cyclostationary.
 - c) *Asynchronous impulsive noise*: This has an unpredictable nature, with no regular occurrence and is mainly due to transients caused by the connection and disconnection of electrical devices. Because of its fitful appearance pattern, from now on it will be referred to as sporadic impulsive noise.
- 2) *Narrowband interference*: This is mostly formed by sinusoidal or modulated signals with different origins: broadcast stations, spurious disturbances caused by electrical appliances with a transmitter or a receiver, etc. Its level usually varies with the time of the day and, as it will be shown in this paper, in some cases, it also varies synchronously with the mains. Hence, some of them can be also treated as cyclostationary.
- 3) *Background noise*. This term includes the remaining noise types not included in the previous categories. It results from the contribution of multiple noise sources of unknown origin. Some of them can be located even outside the considered premises and are coupled via radiation or via conduction. It can be assumed to be cyclostationary, with a level that is strongly dependent on the number and type of electrical devices connected to the network.

At present time, there are still many unknowns related to the aforementioned noise terms. Regarding the background noise, its probability distribution and instantaneous power spectral density (PSD) are usually accomplished without discarding the

Manuscript received April 16, 2009; revised April 8, 2010; accepted May 24, 2010. Date of publication September 13, 2010; date of current version November 17, 2010. This work was supported in part by the Spanish MEC under Project TIC2003-06842.

The authors are with the Communications Engineering Department, University of Málaga, Málaga 29071, Spain (e-mail: jaca@ic.uma.es; diez@ic.uma.es; francis@ic.uma.es; jjsm@ic.uma.es).

Digital Object Identifier 10.1109/TEM.2010.2052463

impulsive components and the narrowband interferences. As a consequence, the resulting probability distribution is clearly non-Gaussian and a quite peaky PSD is obtained [4], [10]. Concerning the impulsive noise, its analysis has been mainly accomplished in the time domain by means of a digital oscilloscope triggered by a peak detector output. The stored data are employed to compute statistics of the interarrival time, pulse width, and pulse amplitude [7], [8]. This procedure has several drawbacks. The major one is that noise impulses are usually masked by other high-level noise components, in particular narrowband interferences. The presence of the remaining noise terms in the captured data presents two additional problems. First, it makes difficult to identify the periodicity of some impulsive components, especially periodic asynchronous ones, which use to have low-energy pulses. Second, it biases the estimation of the pulses width and amplitude. Finally, time-domain discrimination of the three impulsive noise terms is sometimes impossible because pulses from different components overlap. As a consequence, statistics computed in this way are of little use for the development of realistic noise models.

The aim of this paper is the characterization of the different noise terms. The employed methodology, which combines time-domain and frequency-domain techniques, provides both pulse waveforms and repetition rates of the impulsive noise components. A classification of the narrowband interferences according to their PSD and their statistical characteristics, along with results on the probability distribution and the instantaneous PSD of the background noise, are also given. Measurements employed in this paper have been obtained from a campaign performed in three scenarios: in laboratories and offices of a university building, in an apartment of about 80 m², and in a detached house of about 300 m². The number of noise registers exceeds 50, with a similar number of them at the mentioned locations.

Results presented in this paper are particularly helpful for the development of noise models to be employed in the design and optimization of digital communication systems. This is especially applicable to coding schemes, which must be particularly matched to the noise characteristics. Similarly, a good knowledge of the predictable characteristics of some noise components, e.g., periodic asynchronous impulsive ones, can be also employed in the optimization of modulation parameters and receiver structures [11].

The rest of the paper is organized as follows. Section II describes the measurement setup and the common elements of the employed methodology. Section III describes the specific processing utilized in the analysis of each noise term, provides representative examples and summarizes their main characteristics. Concluding remarks are given in Section IV.

II. MEASUREMENT METHODOLOGY

The measurement setup consists of a PC with a 12 bits data acquisition card (DAC). It has a configurable dynamic range and an input impedance of 50 Ω . The sampling frequency is fixed to 50 Msamples/s. The DAC is plugged to the power network outlets through a coupling circuit whose block diagram is shown in Fig. 1, along with the module of its S_{21} and S_{11} .

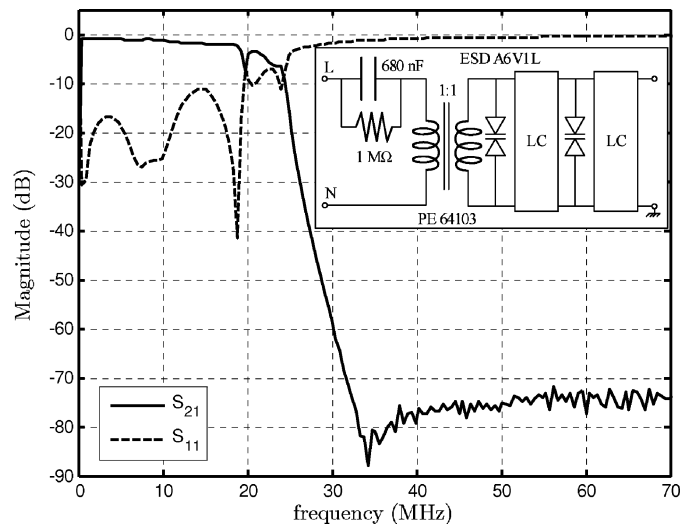


Fig. 1. Coupling circuit scheme and plots of the S_{21} and S_{11} modules.

As seen, it consists of a decoupling capacitor that rejects the mains, a transformer that acts a balun and provides isolation, and the cascade of two identical cells formed by a transient voltage suppression diode and a seven-order Chebyshev bandpass filter. The transmission coefficient has 6-dB cutoff frequencies at 400 kHz and 24 MHz. As seen, the passband ripple is 6 dB and the attenuation at 30 MHz is about 60 dB. The measured total harmonic distortion is higher than 55 dB. Regarding the reflection coefficient of the coupling circuit shown in Fig. 1, it should be mentioned that perfect coupling to the power line network would be unfeasible, even if $S_{11} = 0$ in the passband, because of the frequency selective and time-variant nature of the power line impedance [2].

The performed analysis combines time-domain and frequency-domain techniques. Although the signal processing algorithms used in each case depend on the particularities of the noise component under analysis, a high-resolution spectral analysis based on periodogram averaging is employed in all cases. Because of the cyclostationary nature of most noise terms, this averaging is performed in a cyclic way.

To this end, the captured signal $x(n)$ is registered during C mains cycles, which are real-time transferred to the PC and processed in differed time. Each mains cycle c is divided into L intervals with $N_L = \lfloor T_o/T_s L \rfloor$ samples, where T_o denotes the mains period and T_s the sampling period. Since T_s has been selected to be a submultiple of T_o , the nominal length of each mains cycle is $N_C = T_o/T_s$ samples. However, the mains frequency experiences a time jitter of $\tau(c)$ samples. As a reference, according to the margin established by the European power quality regulation, $\tau(c)$ can be up to 1 ksamples [12]. This time jitter must be taken into account in order to perform the synchronized averaging. Otherwise, after tens of cycles, the averaging will be performed using periodograms that correspond to different intervals of the mains cycle. In this paper, the values of $\tau(c)$ are estimated from a trace of the mains that is intentionally left in $x(n)$. The actual length of the α th cycle is then $N_C + \tau(c)$ samples, and the captured signal during the ℓ th interval of the

c th cycle can be written as

$$x_{c,\ell}(n) = x\left(n + cN_c + \sum_{i=0}^c \tau(i) + \ell N_L\right) \quad (1)$$

with $0 \leq n \leq N_L - 1$. The corresponding periodogram is then computed according to

$$P_c(\ell, k) = \frac{1}{UN_L} \left| \sum_{n=0}^{N_L-1} w(n)x_{c,\ell}(n)e^{-j\frac{2\pi}{N_L}kn} \right|^2 \quad (2)$$

where $w(n)$ is a Hanning window of N_L samples and U is the normalization factor that removes the estimation bias [13]. An estimate of the time- and frequency-sampled version of the noise instantaneous PSD can then be obtained by performing a synchronized averaging of the periodograms in (2)

$$\widehat{S}_N(\ell, k) = \widehat{S}_N(t, f)|_{t=\ell T_s, N_L, f=\frac{k}{T_s N_L}} = \frac{1}{C} \sum_{c=0}^{C-1} P_c(\ell, k) \quad (3)$$

where $C = 234$. The number of time intervals L determines the time and frequency resolution of the estimation. Its selection involves the following tradeoff. An excessively high value of L results in poor frequency resolution that veils the presence of the periodic asynchronous noise terms. On the other hand, an excessively low value of L leads to poor time resolution that does not capture the cyclostationary nature of the background noise. It has been verified that an appropriate value is $L = 15$, which leads to a time and frequency resolution of 1.3 ms and 3 kHz.

The estimated instantaneous PSD in (3) is used as the starting point for the analysis of all noise terms. The next section describes the specific signal processing employed in each case, along with representative results and a summary of their main characteristics.

III. MEASUREMENTS RESULTS

A. Periodic Impulsive Noise Synchronous With the Mains

This noise component appears in a twofold manner: as a series of isolated impulses of considerable duration (up to hundreds of microseconds) and amplitude, and as impulse trains in which the number of impulses and separation between them varies from cycle to cycle. Moreover, impulses within a given train are not equally spaced. The common feature to both terms is that they appear always in the same instant of the mains cycle and have a repetition rate of 50/100 Hz (in Europe). From now onward, the former component will be referred to as type 1 and the latter as type 2. They are typically caused by the nonlinear devices (e.g., thyristors) used in power supplies and motor control circuits. Fig. 2 depicts the time-domain representation of the noise registered in an apartment with a detailed view of the aforementioned components. An amplitude scaled version of the mains has been also drawn as a reference. The increase in the noise level that occurs around 5 and 15 ms is caused by two synchronous narrowband interferences. Type 2 impulses use to be shorter and with lower amplitude than type 1 ones, as shown in Fig. 2.

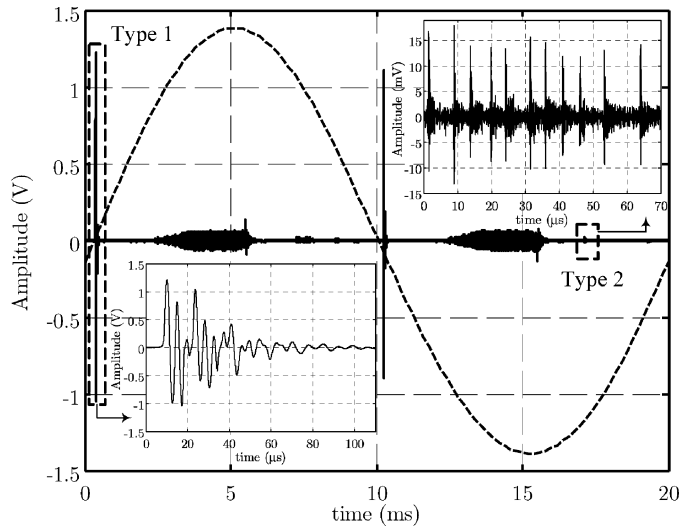


Fig. 2. Noise registered in an apartment during one mains cycle with a detailed view of the periodic synchronous impulsive components. A scaled version of the main is included as a reference.

The procedure employed to obtain pulse waveforms makes use of the estimated instantaneous PSD in (3). Since the resolution of the spectral analysis is insufficient to appreciate the harmonics due to the 50/100 Hz periodicity, the position of these noise components within the mains cycle is detected by identifying frequency selective variations of the level in successive intervals of $\widehat{S}_N(\ell, k)$ (normally higher than 5 dB). Pulses are then extracted by means of a finite-impulse response filter with multiple passbands (one for each of the frequency bands where the instantaneous PSD exhibits important level variations) [13]. Finally, the periodic behavior is verified by correlating them with the overall noise register.

As stated earlier, type 1 impulses usually have large amplitudes. However, the presented procedure is able to obtain pulses whose level difference with respect to the remaining noise terms is much smaller than the ones shown in Fig. 2. Fig. 3(a) shows the noise registered in a detached house during one mains cycle. The presence of the type 1 periodic impulse, along with two of the time intervals in which the instantaneous PSD is estimated, is highlighted. Fig. 3(b) depicts the corresponding instantaneous PSD at time intervals $\ell = 6$, where the impulse is present, and to the previous one, $\ell = 5$. Fig. 3(c) shows the pulse waveform $p(t)$ of the impulse obtained with the proposed methodology, and Fig. 3(d) plots the corresponding normalized energy spectral density (ESD), defined as

$$\text{ESD}(f) = 20 \log_{10} \left(\frac{|P(f)|}{\max\{|P(f)|\}} \right) \quad (\text{dB}) \quad (4)$$

where $P(f)$ is the Fourier transform of $p(t)$ in volts.

Table I summarizes the main parameters of the periodic impulsive noise components that have been measured in the three scenarios. It is interesting to note that, from a communication system perspective, type 2 is generally the most harmful term, despite its lower amplitude, since type 1 impulses are usually located below 1 MHz. The upper and lower bounds shown in Table I reveal that impulses of the same type exhibit a remarkable

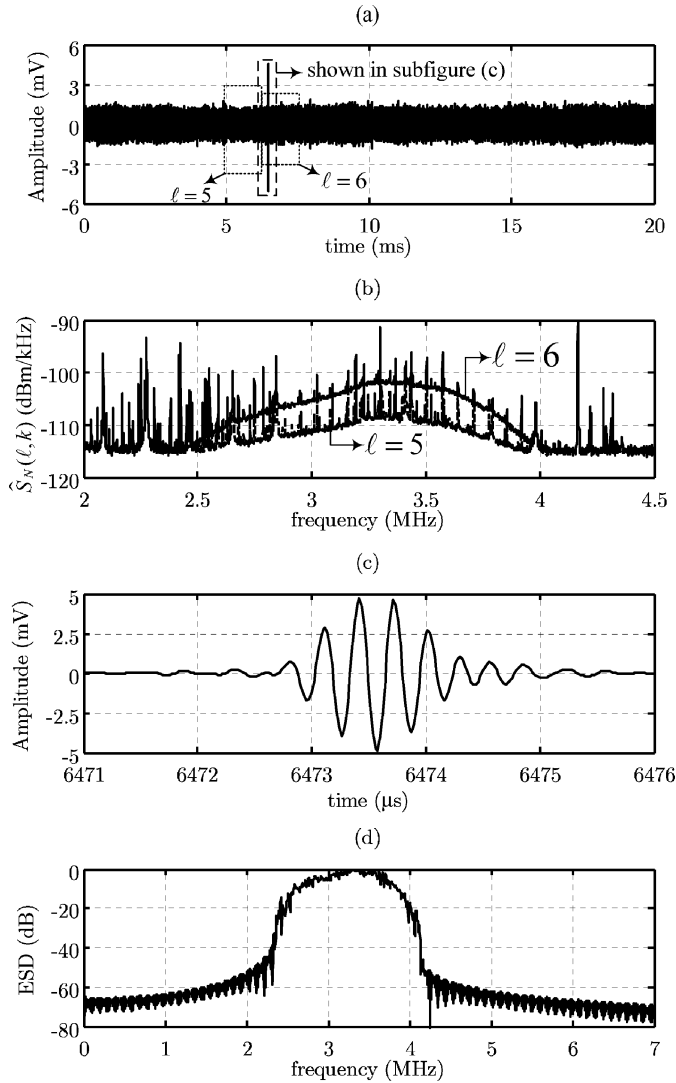


Fig. 3. (a) Noise registered in a detached house during one mains cycle, (b) estimated instantaneous PSD at time intervals $\ell = 6$ and $\ell = 5$, (c) detailed view of the type 1 periodic synchronous pulse waveform, and (d) ESD of the pulse.

disparity of characteristics. This behavior is due to the appliances connected to the power network, whose emitted noise exhibits significant differences even among devices of the same type but produced by different manufacturers.

B. Periodic Impulsive Noise Asynchronous With the Mains

This noise component takes the form of impulse trains whose constituent impulses have repetition rates that are not related to the mains frequency, ranging from approximately 12 up to 217 kHz. Former noise classifications designate this term as asynchronous because of this reason. It has been recently shown that these impulse trains always appear at the same instants of the mains cycle [14], which also makes them to be synchronized with the mains. However, to avoid confusion, the classical nomenclature will be used in this paper. It is also interesting to highlight that this noise component has a common feature with the type 2 periodic synchronous impulsive noise described in the

TABLE I
SUMMARY OF THE PERIODIC SYNCHRONOUS IMPULSIVE NOISE CHARACTERISTICS

Parameter	Type 1	Type 2
Number of impulses within a mains cycle	less than 10	less than 10
Duration	from 2 μs up to 300 μs	train duration up to 500 μs and impulse duration smaller than 1 μs
Amplitude	from 5 mV up to 1.5 Volt	less than 50mV
Central frequency	typically below 500 kHz, occasionally up to 3 MHz	up to 7 MHz
Bandwidth	typically below 250 kHz, occasionally up to 2 MHz	up to 11 MHz

previous section: in both cases, the impulse trains appear at the same instant of the mains cycle. However, the difference is that impulses within a given train of the type 2 periodic synchronous noise are not equally spaced.

According to our measurements, the duration of these impulse trains is always much higher than 1.3 ms, which is the time resolution of the noise instantaneous PSD estimated with $L = 15$. Hence, they will appear in the periodogram as a periodical component will do, i.e., as very narrow peaks whose bandwidth is determined by the main lobe of the Hanning window employed in (2) and whose frequency separation is equal to its repetition rate. The performance of this method is controlled by the value of L . It determines the values of both the minimum repetition rate and impulse train duration that can be detected.

To obtain the pulse waveforms and the repetition rates, a spectral mask $M_\ell^i(k)$ that identifies all the spectral peaks due to the i th periodic asynchronous component of the ℓ th interval is determined according to the algorithm described in [14]. Given that $M_\ell^i(k) = 1$, if the corresponding asynchronous noise term has a spectral peak in k and zero elsewhere, then the pulse waveform can be obtained as

$$p_i(n) = \text{IDFT} \{ M_\ell^i(k) \text{DFT} \{ x_{c,\ell}(n) \} \} \quad (5)$$

where $\text{DFT} \{ \cdot \}$ and $\text{IDFT} \{ \cdot \}$ denote the N_L -point discrete Fourier transform and inverse DFT, respectively.

This procedure is able to retrieve pulse waveforms with very low amplitude that would be undetectable with the traditional measurement procedure based on a digital oscilloscope triggered by a peak detector. Fig. 4 shows an example of this situation. Fig. 4(a) depicts a small interval of the noise captured in an apartment. The y-axis has been scaled according to the amplitudes registered during the first 1.3 ms. This makes it difficult to notice that the term around 1.5 ms is a high-amplitude periodic impulse synchronous with the mains. As seen, there is no visual trace of any periodic asynchronous impulsive component. However, the estimated PSD for this interval, shown in Fig. 4(b), clearly reveals its presence. The proposed methodology gives

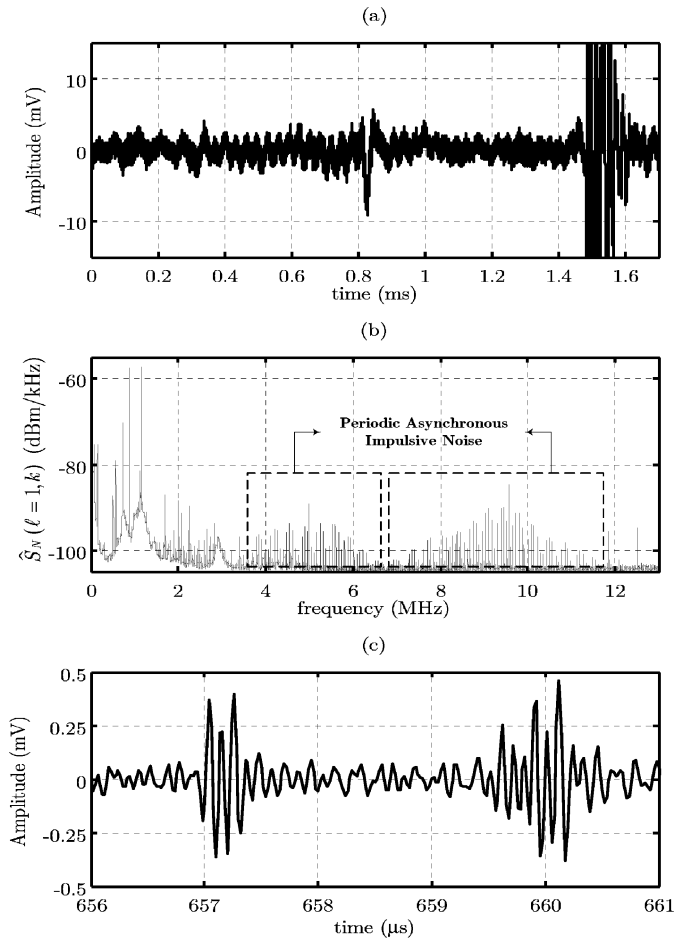


Fig. 4. (a) Time-domain representation of the noise registered in an apartment, (b) estimated PSD of the first 1.3 ms, and (c) pulse waveform of the existing periodic asynchronous noise component.

the pulse waveform, drawn in Fig. 4(c), which consists of a set of two impulses with a repetition rate of 70 kHz.

Fig. 5(a) depicts an example of low-repetition-rate periodic asynchronous impulsive noise registered in a university laboratory. It is basically composed of two short pulses (duration around 1 μ s) that alternate their polarity once per period. The repetition rate of this component is 26.3 kHz, which is well below the range typically assigned in the literature to this noise type. Fig. 5(b) shows the ESD corresponding to the first impulse in Fig. 5(a).

Fig. 6 shows an example of periodic asynchronous impulsive noise with high frequency components. Fig. 6(a) depicts the time-domain waveform, which is composed of a higher amplitude and a low-amplitude pulse that repeats with 48.93 kHz, and Fig. 6(b) shows the corresponding ESD.

Periodic asynchronous impulse terms usually appear only in certain instants of the mains cycle. A common appearance pattern is composed of two impulse trains symmetrically located within the mains cycle. A pattern in which the trains appear both in the vicinity of the zero crossings or also around the minimum and maximum mains voltage values. Nevertheless, there is a great variety of them, and situations in which some

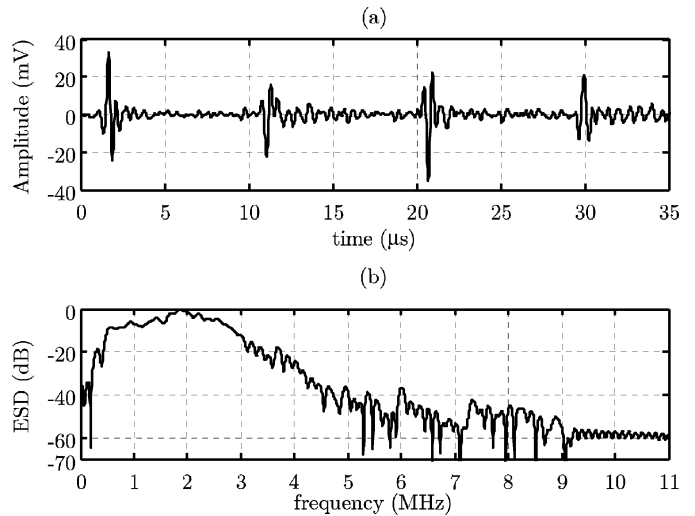


Fig. 5. (a) Time-domain representation of a low-repetition rate periodic asynchronous impulsive noise and (b) ESD of the first impulse.

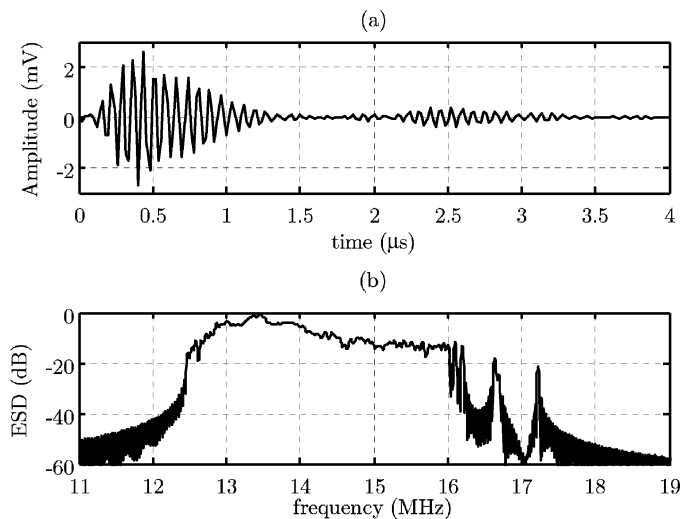


Fig. 6. (a) Time-domain representation and (b) ESD of a periodic asynchronous impulsive noise with high frequency components.

noise components are present during the whole mains cycle but with different amplitudes have been also found [14]. In all cases, impulses are generally present in at least 50% of the mains cycle duration. Table II summarizes the main characteristics of the measured periodic asynchronous impulsive noise.

C. Sporadic Impulsive Noise

This is the most unpredictable impulsive noise term. Two types of sporadic components have been observed. The first one consists of isolated impulses with considerable amplitudes and widths, and from now on these will be referred to as type 1. The second one takes the form of impulse trains with arbitrary separation between the constituent pulses, and from now on these will be denoted as type 2. These constituent pulses typically have lower amplitude and smaller duration than those of the first type.

TABLE II
SUMMARY OF THE PERIODIC ASYNCHRONOUS IMPULSIVE NOISE CHARACTERISTICS

Parameter	Value
Number of different components in a mains cycle	one or none in weakly disturbed scenarios and more than 3 in highly disturbed ones
Appearance pattern	present all the time, 2 states (on/off) per mains cycle, 4 states (on/off) per mains cycle & others
Duration	typically less than 1.5 μ s, occasionally up to 10 μ s
Amplitude	typically less than 4 mV, occasionally up to 40 mV
Repetition rates	12.6 kHz, 15.6 kHz, 26.3 kHz, 48.9 kHz, 56.5 kHz, 59.1 kHz, 70 kHz, 90.1 kHz and 217.2 kHz
Central frequency	from 2 MHz up to 13 MHz
Bandwidth	from 2 MHz up to 13 MHz

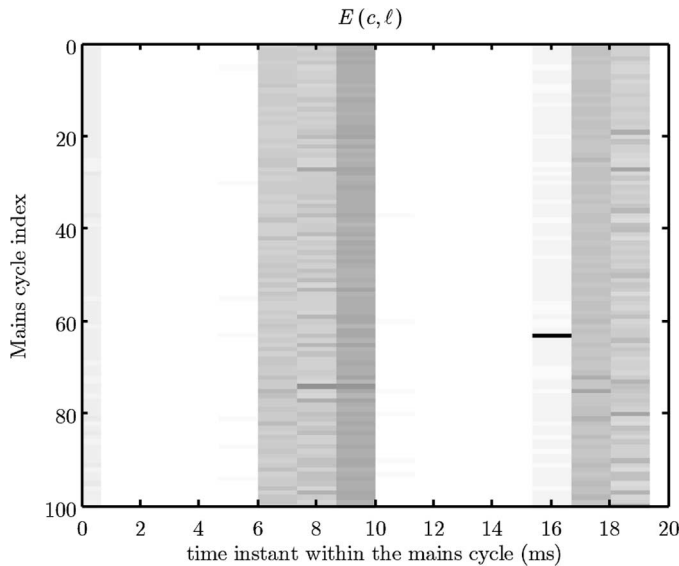


Fig. 7. Spectrogram of the energy computed over 100 mains cycles with $L = 15$ intervals per mains cycle.

In all cases, those intervals of the mains cycle containing these noise types have larger energy than the remaining ones. Hence, the procedure employed to detect them divides the mains cycle into L intervals and computes their energy, leading to

$$E(c, \ell) = \sum_{n=0}^{N_L-1} |x_{c,\ell}(n)|^2. \quad (6)$$

Then, high energy intervals that do not appear in successive cycles are searched.

Fig. 7 depicts results obtained when computing the energy of 100 mains cycles divided into $L = 15$ intervals. As seen, cyclostationary noise components are clearly identifiable by the vertical stripes around 0, 8, and 18 ms. A type 1 sporadic impulsive noise with very high energy can be observed around 16

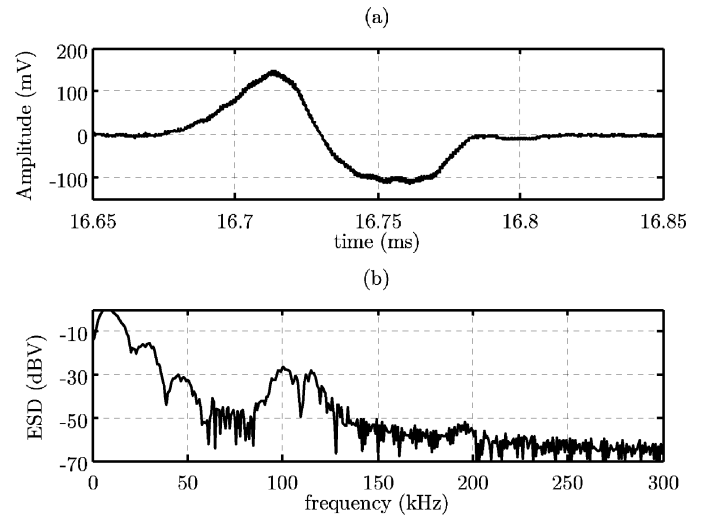


Fig. 8. (a) Time-domain representation and (b) ESD of the sporadic impulsive noise identified in Fig. 7.

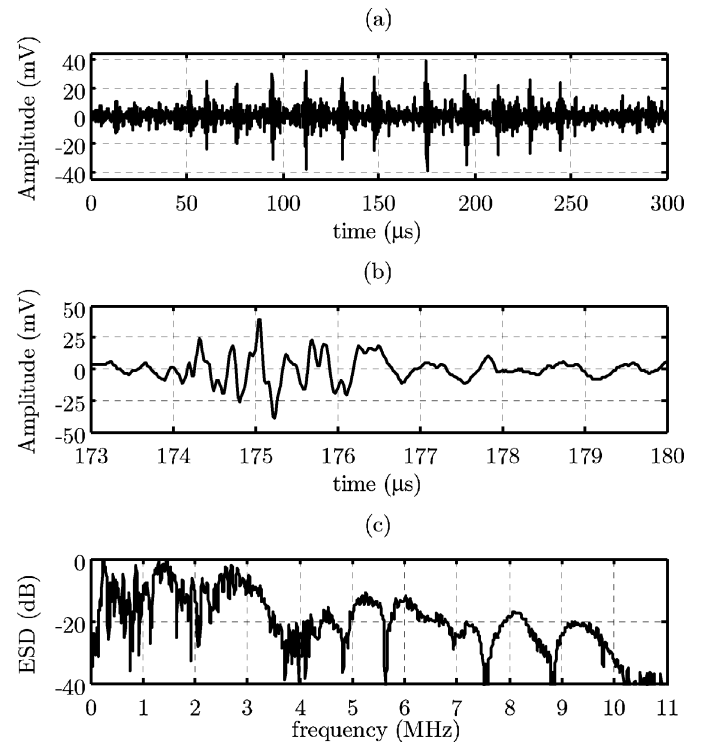


Fig. 9. (a)–(b) Time-domain representation and (c) ESD of a type 2 sporadic impulsive noise.

ms in the 64th cycle. Fig. 8 displays the corresponding pulse waveform and its ESD.

Fig. 9 shows an example of type 2 sporadic impulsive noise. Fig. 9(a) displays the impulse train, Fig. 9(b) shows a detail of the impulse with higher amplitude (although all of them have essentially the same waveform), and Fig. 9(c) depicts its ESD. As seen, type 2 impulses have lower amplitude and higher frequency components. Table III summarizes the main characteristics of both sporadic noise types.

TABLE III
SUMMARY OF THE SPORADIC IMPULSIVE NOISE CHARACTERISTICS

Parameter	Type 1	Type 2
Duration	from 15 μ s up to 150 μ s	less than 20 μ s
Amplitude	from 20 mV up to 150 mV	from 3 mV up to 50 mV
Central frequency	typically below 1 MHz	up to 7 MHz
Bandwidth	typically below 1 MHz	up to 11 MHz

Isolated sporadic impulses can be automatically detected by means of (6) and a single threshold that depends on the background noise. However, more complicated situations arise when they appear within the vertical stripes (i.e., simultaneously with periodic noise components), or within the time interval in which the cyclostationary background noise level exhibits a significant increment. These cases may require additional actions like the computation and comparison of (6) for different values of L , or a detailed analysis of the impulses that appear in the time interval.

Previous analyses, in which interarrival and amplitude distributions are computed without differentiating between the two periodic noise terms, show that impulses with greater width and amplitude have higher probability in weakly disturbed scenarios [7]. This can be easily explained according to the results presented in this paper. Measurements indicate that the difference between weakly and highly disturbed scenarios, in terms of noise pulses, is essentially due to the number of periodic asynchronous impulsive terms. Sporadic impulses and periodic synchronous terms are generally the only impulsive components in weakly disturbed environments. Hence, according to data presented in Tables I–III, most of the impulses registered in these situations have large amplitude and duration.

D. Narrowband Interference

This disturbance type is easily detected in the estimated instantaneous PSD because of its significant level over the background noise and, in general, over the remaining noise terms. They can be classified according to the shape of their PSD into the following categories:

- 1) *Interference with multiple discrete frequency components:* The PSD of this interference consists of several equally spaced narrowband components (less than 5 kHz bandwidth). However, contrary to the peaks due to periodic asynchronous terms, they are not harmonically related, i.e., denoting by f_j , with $j = 0, 1, \dots$, the frequencies of the spectral peaks, it happens that $f_j - f_{j-1} = f_{j+1} - f_j$ but there is no f_0 that satisfies $f_j = pf_0$, for $j = 0, 1, \dots$ and $p \in \mathbb{N}^+$. They are usually located above 4 MHz and frequency spacings up to 50 kHz have been observed. Fig. 10(a) shows the estimated PSD of an interference of this type. As seen, it has the shape of the double-sideband modulation of a periodic signal. Fig. 10(b) depicts its corresponding time-domain waveform, obtained by applying a bandpass filter to the noise register.

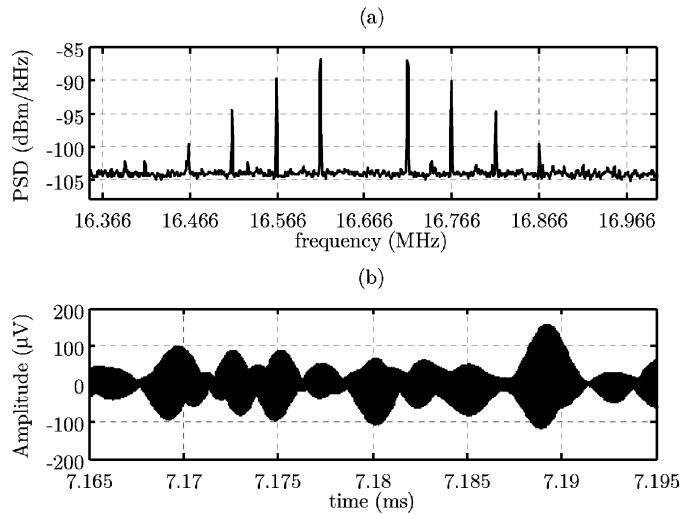


Fig. 10. (a) PSD of interference with multiple discrete frequency components and (b) its corresponding time-domain waveform.

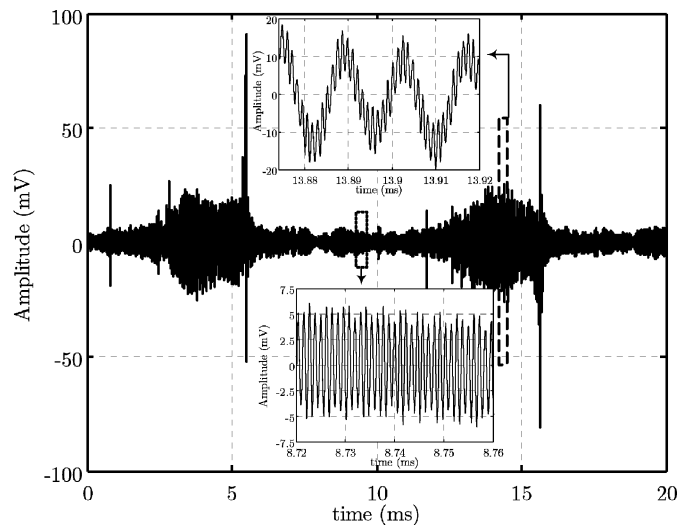


Fig. 11. Noise registered in an apartment during one mains cycle with detailed view of two narrowband interferences.

- 2) *Interference with one frequency component:* The PSD of this interference consists of a single-narrowband term (bandwidth below 20 kHz) and a significant level over the background noise (even more than 30 dB). They can be typically found below 2 MHz and above 20 MHz. Interference from commercial AM radio stations is an example of this category.

Alternately, interference can be classified according to their statistical properties into:

- 1) *Stationary:* They can be composed of multiple equally spaced narrowband components or just a single term, but their levels do not change along the mains cycle. Most of the registered interference fall within this group.
- 2) *Cyclostationary:* This interference can be also composed of multiple frequency terms or a single one. However, its distinctive feature is its synchronous character with the mains. Fig. 11 shows the time-domain representation of

a noise register that contains this type of interference. It depicts the detailed view of a 76-kHz-cyclostationary narrowband interference that appears just before the two periodic synchronous impulses with highest amplitude. The superimposed effect of AM interference with a carrier frequency of 882 kHz and smaller amplitude can also be observed. The cyclostationary behavior of the 76 kHz interference is corroborated by the zoomed region around 8 ms, where only the AM interference is present. As shown in Fig. 11, this interference usually precedes the periodic synchronous impulses.

E. Background Noise

The analysis of the cyclostationary background noise is aimed at estimating its instantaneous PSD, $\hat{S}_{BN}(\ell, k)$. To this end, the spectral peaks caused by the periodic asynchronous impulsive noise components and the narrowband interference must be removed. This objective is achieved by applying the following algorithm to each time interval ℓ :

- 1) *Estimate the instantaneous PSD of the registered noise:* An estimate of the noise instantaneous PSD $\hat{S}_N(\ell, k)$ is obtained according to (3) with $L = 15$.
- 2) *Determine the set of frequencies corresponding to the spectral peaks in $\hat{S}_N(\ell, k)$:* Denoting by k_ℓ^i , with $i = 0, 1, \dots$, the frequencies where $\hat{S}_N(\ell, k)$ has a spectral peak, the output of this phase is the set $K_\ell = \{k_\ell^0, k_\ell^1, \dots\}$.
- 3) *Eliminate the spectral peaks in $\hat{S}_N(\ell, k)$:* The objective of this step is to generate a new PSD $\tilde{S}_N(\ell, k)$ equal to $\hat{S}_N(\ell, k)$ but with no trace of the spectral peaks due to the narrowband interference and to the periodic asynchronous impulsive components. To this aim, the values of $\hat{S}_N(\ell, k)$ for $k \in K_\ell$ are replaced by the minimum value taken by $\hat{S}_N(\ell, k)$ in an interval centered in k

$$\tilde{S}_N(\ell, k) = \begin{cases} \hat{S}_N(\ell, k) & k \notin K_\ell \\ \min_{\kappa=k-W/2 \dots k+W/2} \{\hat{S}_N(\ell, \kappa)\} & k \in K_\ell. \end{cases} \quad (7)$$

The interval length W determines the bandwidth of the minimum filtering employed in (7). Its selection involves the following tradeoff. On the one hand, it must be larger than the bandwidth of both, the spectral peaks due to the periodic asynchronous impulsive noise terms, which is 3 kHz, and the narrowband interferences that appear in the analyzed frequency band, which are about 20 kHz. On the other hand, it must be smaller than the coherence bandwidth of the instantaneous PSD. In this paper, the selected value for W results in a bandwidth of approximately 30 kHz.

- 4) *Smooth the staircase shape of $\tilde{S}_N(\ell, k)$:* The processing in (7) gives a staircase behavior to $\tilde{S}_N(\ell, k)$ in the vicinity of $k \in K_\ell$. To remove it, a weak low-pass filter is applied to $\tilde{S}_N(\ell, k)$, yielding to an estimation of the background noise $\hat{S}_{BN}(\ell, k)$.

Fig. 12 depicts the $\hat{S}_N(\ell, k)$ of the noise registered in a university laboratory. It corresponds to a heavily disturbed scenario,

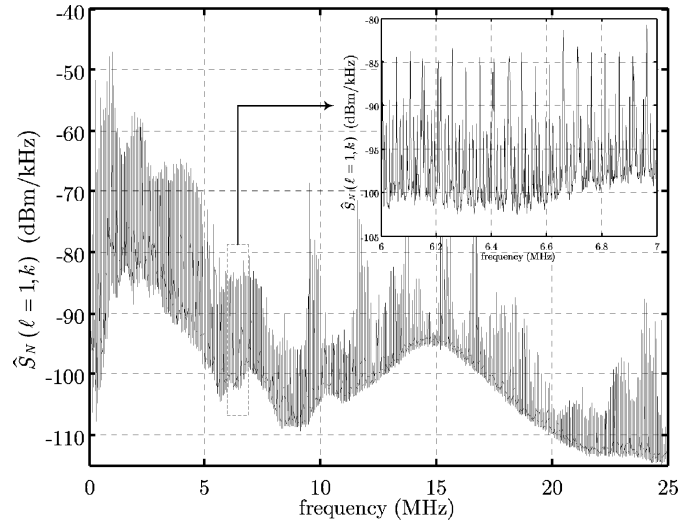


Fig. 12. Estimated PSD of the noise registered in a university laboratory.

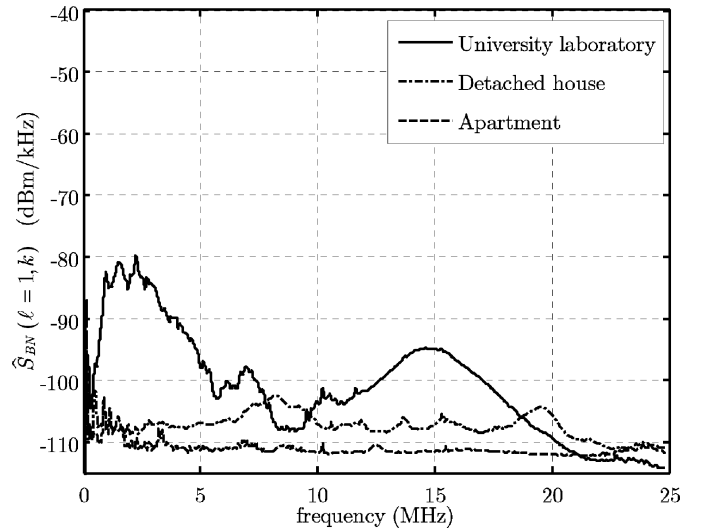


Fig. 13. Background noise PSD obtained from Fig. 12 and from the noise registered in a detached house and in an apartment.

with a lot of periodic asynchronous components. A zoom of the frequency band between 6 and 7 MHz has been included to better appreciate them.

Fig. 13 shows the values of $\hat{S}_{BN}(\ell, k)$ corresponding to the PSD shown in Fig. 12. Additionally, the estimates of the background noise obtained in a detached house and in an apartment have also been included. As seen, the background noise PSD of the noise registered in the university laboratory does not fit the simple exponential models proposed in previous works [4], [15]. These models are appropriate for weakly disturbed scenarios and, in some cases, for medium disturbed ones. However, they do not capture the spectral richness of the noise existing in highly disturbed environments.

The cyclostationary nature of the background noise can be observed in Fig. 14. It depicts the estimated PSD of the background noise registered in a university laboratory at three different time intervals within the mains cycle. As seen, differences of about

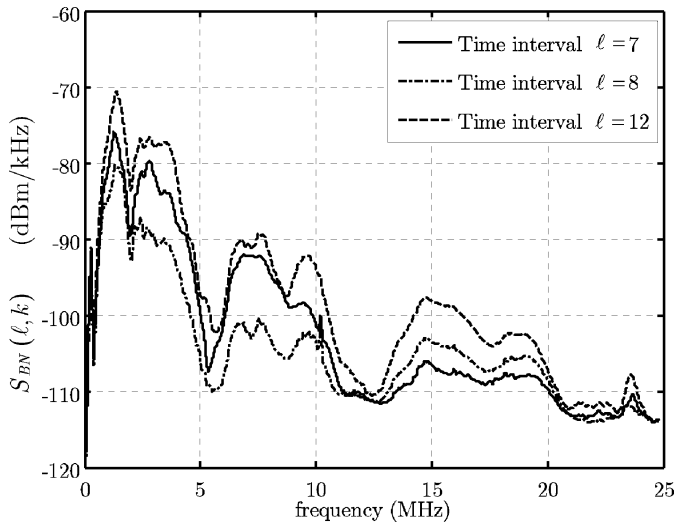


Fig. 14. Estimated PSD of the background noise registered in a university laboratory.

10 dB occur in many frequency bands. This cyclostationary behavior has been observed in all the scenarios. However, it has been more frequently found, and with higher level differences, in highly disturbed environments.

The presented algorithm cannot be applied to estimate the background noise PSD of those intervals with periodic synchronous impulsive noise, or at least not in the frequency band occupied by them. The reason is that the operation in (7) does not remove them from the PSD because of the insufficient resolution of the spectral analysis. This is not a serious impairment because these impulses are time localized and occupy only a small percentage of the mains cycle. Moreover, if these impulses are removed by means of a notch filter, the background noise PSD in the remaining band can also be estimated in these intervals by means of the proposed method.

E. Noise Probability Density Function

According to the noise components described up to now, it is clear that broadband PLC noise does not have a Gaussian nature when considered as a whole. This fact has been already reported in the literature [4] and is a consequence of the presence of multiple impulsive noise components and high-level narrowband interference. On the other hand, the background noise results from the contribution of a large number of independent sources. Therefore, it is expected to have a Gaussian distribution. This section investigates this end by estimating the probability density function (PDF) of the samples amplitude at multiple time intervals of the mains cycle. To obtain a higher time resolution, L is fixed to a much higher value than in previous sections: $L = 976$. The estimated PDF of the ℓ th interval is then obtained from the samples of $x_{c,\ell}(n)$ for $c = 0 \dots C - 1$.

Fig. 15 shows some of the PDFs estimated over the noise register acquired in a detached house. Depicted curves correspond to the logarithm of the normalized PDFs computed at 14 intervals within the mains cycle. To facilitate the comparison among PDFs with different noise variance, curves are normalized to

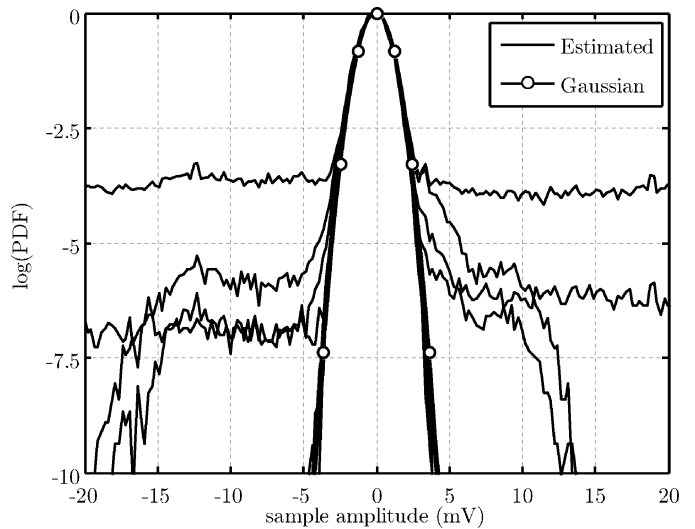


Fig. 15. Estimated PDFs of the noise registered in a detached house at different time intervals.

their peaks, while the logarithm is computed to obtain higher resolution at the tails of the Gaussian curves.

As seen, there are four PDFs that exhibit higher probabilities than a normally distributed variable for extreme values. This non-Gaussian nature is caused by the presence of impulsive noise components within the analyzed interval. The asymmetry of the PDF in these cases is caused by the asymmetry of the voltage amplitudes in periodic synchronous impulses, as can be observed in Fig. 2. The remaining ten curves correspond to intervals with neither trace of noise impulses nor narrowband interferences. They match the Gaussian curve (which is included as a reference) so closely that they are indistinguishable. Hence, it can be concluded that the background noise is Gaussian.

IV. CONCLUSION

This paper has presented a detailed analysis of the indoor broadband power-line noise components. The employed methodology combines time-domain techniques with a high-resolution spectral analysis based on periodogram averaging that captures the cyclostationary nature of most noise terms. The study relies on a measurement campaign performed over more than 50 noise registers in three different scenarios.

Concerning the impulsive noise, it has been shown that periodic synchronous terms have a twofold nature: a series of isolated impulses and impulse trains in which the number of impulses and separation between them varies from cycle to cycle. Both impulse types always appear in the same instant of the mains cycle, but the latter use to be shorter and with lower amplitude than the first ones. On the other hand, the former impulses typically occupy the frequency band below 1 MHz, while the latter can be found in frequency bands up to 11 MHz. Similarly, the analysis of the periodic asynchronous noise has revealed that they also exhibit a synchronous behavior with the mains. Repetition rates from 12.6 up to 217.2 kHz have been measured. Similarly, a procedure to extract sporadic impulsive noise, which is the most unpredictable term, has been presented.

Examples of pulse waveforms and their corresponding energy spectral densities have been given in all cases.

A classification of the narrowband interference according to its PSD and its statistical behavior has also been given. It has been shown that some of them exhibit a cyclostationary behavior. Finally, a procedure to compute the background noise PSD has been presented. It has been demonstrated that the classical exponential model does not capture the spectral richness of the heavily disturbed scenarios. It has also been shown that, according to the accomplished measurements, the background noise has a Gaussian distribution.

ACKNOWLEDGMENT

The authors would like to thank the Associate Editor P. Wilson and the anonymous reviewers for their thorough revision of the manuscript and their valuable comments and suggestions.

REFERENCES

- [1] H. Philipps, "Performance measurements of power-line channels at high frequencies," in *Proc. Int. Symp. Power Line Commun. Appl. (ISPLC)*, 1998, pp. 229–237.
- [2] F. J. Cañete, J. A. Cortés, L. Díez, and J. T. Entrambasaguas, "Analysis of the cyclic short-term variation of indoor power line channels," *IEEE J. Sel. Areas Commun.*, vol. 24, no. 7, pp. 1327–1338, Jul. 2006.
- [3] F. J. Cañete, L. Díez, J. A. Cortés, and J. T. Entrambasaguas, "Broadband modelling of indoor power-line channels," *IEEE Trans. Consum. Electron.*, vol. 48, no. 1, pp. 175–183, Feb. 2002.
- [4] T. Esmailian, F. R. Kschischang, and P. G. Gulak, "In-building power lines as high-speed communication channels: Channel characterization and a test channel ensemble," *Int. J. Commun.*, vol. 16, pp. 381–400, Jun. 2003.
- [5] S. Galli and T. C. Banwell, "A deterministic frequency-domain model for the indoor power line transfer function," *IEEE J. Sel. Areas Commun.*, vol. 24, no. 7, pp. 1304–1316, Jul. 2006.
- [6] Y. Hirayama, H. Okada, T. Yamazato, and M. Katayama, "Noise analysis on wide-band PLC with high sampling rate and long observation time," in *Proc. Int. Symp. Power Line Commun. Appl. (ISPLC)*, 2003, pp. 142–147.
- [7] M. Zimmermann and K. Dostert, "Analysis and modeling of impulsive noise in broadband powerline communications," *IEEE Trans. Electromagn. Compat.*, vol. 44, no. 1, pp. 249–258, Feb. 2002.
- [8] V. Degardin, M. Lienard, A. Zeddou, F. Gauthier, and P. Degauque, "Classification and characterization of impulsive noise on indoor power line used for data communications," *IEEE Trans. Consum. Electron.*, vol. 48, no. 4, pp. 913–918, Nov. 2002.
- [9] D. Liu, E. Flint, B. Gaucher, and Y. Kwark, "Wide band AC power line characterization," *IEEE Trans. Consum. Electron.*, vol. 45, no. 4, pp. 1087–1097, Nov. 1999.
- [10] H. Meng, Y. L. Guan, and S. Chen, "Modeling and analysis of noise effects on broadband power-line communications," *IEEE Trans. Power Del.*, vol. 20, no. 2, pp. 630–637, Apr. 2005.
- [11] R. García, L. Díez, J. A. Cortés, and F. J. Cañete, "Mitigation of cyclic short-time noise in indoor power-line channels," in *Proc. IEEE Int. Symp. Power Line Commun. Appl. (ISPLC)*, Mar. 2007, pp. 396–400.
- [12] CENELEC EN 50160, "Voltage Characteristics of Electricity Supplied by Public Distribution Systems," 1999.
- [13] A. Oppenheim, R. Schaffer, and J. Buck, *Discrete-Time Signal Processing*, 2nd ed. Englewood Cliffs, NJ: Prentice-Hall, 1999.
- [14] J. A. Cortés, L. Díez, F. J. Cañete, and J. López, "Analysis of the periodic impulsive noise asynchronous with the mains in indoor PLC channels," in *Proc. IEEE Int. Symp. Power Line Commun. Appl. (ISPLC)*, Mar./Apr. 2009, pp. 26–30.
- [15] D. Benyoucef, "A new statistical model of the noise power density spectrum for powerline communication," in *Proc. Int. Symp. Power-Line Commun. Appl. (ISPLC)*, Mar. 2003, pp. 136–141.



José Antonio Cortés received the M.S. and Ph.D. degrees in telecommunication engineering in 1998 and 2007, respectively, from the University of Málaga, Málaga, Spain.

In 1998, he received a fellowship from Alcatel Citesa. In 1999, he worked for Alcatel España R&D. This same year he joined the Communication Engineering Department of the University of Málaga, where he is currently working as an Associate Professor. From 2000 to 2002, he collaborated with the Nokia System Competence Team in Málaga. His research interests include digital signal processing for communications, mainly focused on synchronization and transmission techniques for high-speed power line communications.



Luis Díez received the M.S. and Ph.D. degrees from the Polytechnic University of Madrid, Madrid, Spain, in 1989 and 1995, respectively, both in telecommunications engineering.

In 1984, he joined Fujitsu-España R&D center. From 1987 to 1997, he was with the Department of Signals, Systems, and Radiocommunication, Polytechnic University of Madrid. Since 1997, he has been with the Communications Engineering Department, University of Málaga, where he is currently working as an Associate Professor. He has great experience in technical aspects of digital communication, e.g., synchronization, adaptive signal processing, modulation, coding and multiple access.



Francisco Javier Cañete received the M.S. and Ph.D. degrees in telecommunication engineering in 1996 and 2004, respectively, from the University of Málaga, Málaga, Spain.

In 1996, he worked for the Empresa Nacional de Ingeniería y Tecnología (INITEC). In 1997, he worked for Alcatel España R&D Department. Since 1998, he works for the Communications Engineering Department, University of Málaga, where he is currently an Associate Professor. From 2000 to 2001, he also collaborated with the Nokia System Competence Team in Málaga. His research activity is focused on digital signal processing for communications, including channel modelling and transmission techniques for wireless and power-line communication systems.



Juan José Sánchez-Martínez received the B.S. and the M.S. degrees in telecommunication engineering in 2003 and 2006, respectively, both from the University of Málaga, Málaga, Spain. In 2006, he joined the Communications Engineering Department, University of Málaga, where is currently working towards the Ph.D.

His research interests are focused on signal processing for digital communications and on real-time implementation of signal processing algorithms on field-programmable gate array.